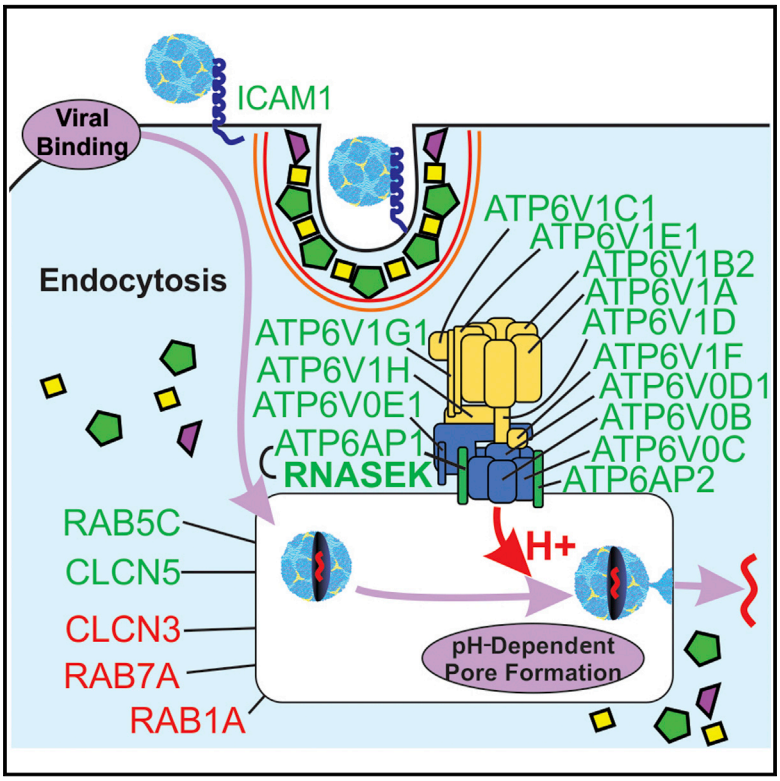
Article

Cell Reports

RNASEK Is a V-ATPase-Associated Factor Required for Endocytosis and the Replication of Rhinovirus, Influenza A Virus, and Dengue Virus

Graphical Abstract



Highlights

- Host proteins that modulate HRV replication were found by using MORR screens
- RNASEK is needed for the replication of HRV, influenza A virus, and dengue virus
- RNASEK localizes to the cell surface and endosomal pathway along with the V-ATPase
- RNASEK is needed for endocytosis, and its loss produces enlarged clathrin-coated pits

Authors

Jill M. Perreira, Aaron M. Aker, George Savidis, ..., Annick Gauthier, Michael Franti, Abraham L. Brass

Correspondence

abraham.brass@umassmed.edu

In Brief

Perreira et al. screened multiple orthologous RNAi reagents and identified host proteins that modulate human rhinovirus (HRV) replication. They found that RNASEK is needed for the replication of HRV, influenza A virus, and dengue virus, associates with the vacuolar ATPase (V-ATPase), and is required for endocytosis.

Perreira et al., 2015, Cell Reports *12*, 850–863
August 4, 2015 ©2015 The Authors
http://dx.doi.org/10.1016/j.celrep.2015.06.076

CellPress

OPEN ACCESS
CellPress

Cell Reports
Article

RNASEK Is a V-ATPase-Associated Factor Required for Endocytosis and the Replication of Rhinovirus, Influenza A Virus, and Dengue Virus

Jill M. Perreira,[1,3] Aaron M. Aker,[1,3] George Savidis,[1,3] Christopher R. Chin,[1] William M. McDougall,[1] Jocelyn M. Portmann,[1] Paul Meraner,[1] Miles C. Smith,[1] Motiur Rahman,[1] Richard E. Baker,[1] Annick Gauthier,[2] Michael Franti,[2] and Abraham L. Brass[1,*]

[1]Microbiology and Physiological Systems Department, University of Massachusetts Medical School, University of Massachusetts, Worcester, MA 01655, USA

[2]Boehringer Ingelheim Pharmaceuticals, Inc., 900 Ridgebury Road, Ridgefield, CT 06877, USA

[3]Co-first author

*Correspondence: abraham.brass@umassmed.edu

http://dx.doi.org/10.1016/j.celrep.2015.06.076

This is an open access article under the CC BY-NC-ND license (http://creativecommons.org/licenses/by-nc-nd/4.0/).

SUMMARY

Human rhinovirus (HRV) causes upper respiratory infections and asthma exacerbations. We screened multiple orthologous RNAi reagents and identified host proteins that modulate HRV replication. Here, we show that RNASEK, a transmembrane protein, was needed for the replication of HRV, influenza A virus, and dengue virus. RNASEK localizes to the cell surface and endosomal pathway and closely associates with the vacuolar ATPase (V-ATPase) proton pump. RNASEK is required for endocytosis, and its depletion produces enlarged clathrin-coated pits (CCPs) at the cell surface. These enlarged CCPs contain endocytic cargo and are bound by the scissioning GTPase, DNM2. Loss of RNASEK alters the localization of multiple V-ATPase subunits and lowers the levels of the ATP6AP1 subunit. Together, our results show that RNASEK closely associates with the V-ATPase and is required for its function; its loss prevents the early events of endocytosis and the replication of multiple pathogenic viruses.

INTRODUCTION

Human rhinovirus (HRV) causes an estimated 50% of common colds and is a major precipitant of asthma and chronic obstructive pulmonary disease flares (Johnston et al., 1995; Seemungal et al., 2001). The three species of HRV (A, B, and C) are non-enveloped members of the picornaviridae family and contain a single stranded positive sense RNA genome that encodes for 11 proteins (Simmonds et al., 2010). The serotype-dependent binding of HRV-A and-B to either of two host receptors, ICAM1 (major group viruses) or LDLR (or LDLR-related, minor group), triggers the endocytosis of the viral-receptor complex. Upon entering acidified endosomes, HRV's capsid undergoes a conformational change leading to the formation of a trans-endosomal membrane pore through which the viral genome enters the cytosol. Having gained access to the host cell's resources, the viral genome undergoes translation into a polyprotein, which is processed by the viral protease into both structural and non-structural components. The 5′ UTR of the viral genome possesses an internal ribosomal entry site with specific secondary structure essential for mediating efficient translation. Once liberated from the polyprotein, the viral polymerase synthesizes both anti-sense and sense viral genomes, the latter of which are packaged into the viral capsid assembly to be released upon cell lysis.

To elucidate the role of host proteins in HRV replication, we undertook multiple orthologous RNAi reagent (MORR) genetic screens, followed by a traditional validation strategy. siRNA screens have been useful for investigating host-virus interactions; however, they are hampered by prevalent false positives and false negatives. To offset these shortcomings, we performed parallel MORR screens and integrated the datasets by repurposing an existing RNAi analysis program, RIGER (Luo et al., 2008). RIGER produces a collective phenotypic significance score for each host factor tested in the screen by collectively assessing the screening datasets; this determines what the likelihood is of a gene contributing to the phenotype of interest. To further limit false positives, we used gene-expression filtering to remove candidates that were not expressed in the cells used for the screen. This comprehensive screening effort identified both known (Cherry et al., 2005, 2006) and multiple previously unappreciated factors required by HRV. Among the new HRV host factors (HRV-HFs), the transmembrane protein, RNASEK (Economopoulou et al., 2007; Kiritsi et al., 2012), was required for the replication of multiple HRV serotypes. RNASEK was also needed for the replication of influenza A (IAV) virus and influenza B virus, flaviviruses (dengue virus [DENV] serotypes 2, 3, and 4) and the yellow fever vaccine-strain virus (YF17D), as well as pseudoparticles expressing the vesicular stomatitis virus (VSV)-g protein.

Here we show that RNASEK localized in part to the cell surface and endosomes and proteomic studies demonstrated it associates with the V-ATPase. Depletion of RNASEK decreased clathrin-mediated and non-clathrin-mediated endocytosis and

resulted in the formation of enlarged clathrin-coated pits (CCPs) at the cell surface. Endo-lysosomal acidity was increased with loss of either RNASEK or the V-ATPase, but was lowered with the coordinated silencing of a second proton pumping complex, the P-ATPase, uncovering a functional redundancy. RNASEK was also required for maintaining the levels of both cell-wide and plasma membrane-associated V-ATPase compartments. Together these data reveal that RNASEK is required for V-ATPase function, the early events of endocytosis, and the replication of multiple pathogenic viruses.

RESULTS

Functional Genomic Screens for HRV-HFs

We screened for HRV-HFs by transfecting arrayed siRNA libraries into H1-HeLa cells that endogenously express ICAM1. After 72 hr, the cells were infected with HRV14 (Figure 1A). At 12 hr after infection, the cells were stained using a monoclonal antibody directed against HRV14's V1 CA protein (Che et al., 1998) and stained for DNA. Cell number and percent infection were determined for each well. Positive control siRNAs were against ICAM1 or ATP6V0B (Figure 1B).

This platform was used to screen four RNAi libraries: Silencer Select (21,584 siRNA pools, Ambion), esiRNA (15,300 siRNA pools, Sigma), SMARTpool (17,877 siRNA pools, Dharmacon), and the SMARTpool RefSeq27 Reversion Human 5 subgenomic replacement siRNA library: (SMART-Rev, 4,506 siRNA pools, Dharmacon; Figure 1C; Table S1). These libraries were selected because of their complementary design strategies and collective broad coverage. A comparison of >1,000 siRNA pools from the Silencer Select and SMARTpool libraries demonstrated <5% similar siRNAs showing that the reagents are largely orthologous.

siRNA pools were designated as HRV-HFs if the percentage of infected cells was $\leq$50% or $\geq$150% of the plate mean and cell number was $\geq$40% of the plate mean. Selected HRV-HF candidate pools were validated by independently testing the individual oligos from each pool (Table S1). To increase utility, the majority of the validation round candidates did not include enriched complex genes (i.e., ribosomal subunits) or known HRV-HFs, but instead were chosen because they had little classification and no known association with HRV. In the validation datasets, pools with two or more siRNAs that met the above criteria were deemed higher confidence because such results are more likely to be caused by depletion of the intended target (Echeverri et al., 2006).

HRV-HF Pathways and Complexes

The screens identified several pathways and complexes whose components scored across the four primary screen datasets (Figure S1A). For the V-ATPase, a strong viral dependency was seen for both the V_1 and V_0 subcomplex genes (eight of eight and four of five genes, respectively, found in two or more screens; Figure 1D; Table S2). Among the 24 V-ATPase proteins, there were 9 that did not score as HRV-HFs in any of the screens (Table S2). In addition to host factors required for HRV replication (dependency factors (DFs), we also detected complexes and pathways whose loss enhanced viral infection (competitive factors [CFs]; Tables S1 and S2).

HRV-HF MORR Screens Have False Positives and False Negatives

In general, a comparison of candidate lists from similar siRNA screens shows significant overlap in complexes and pathways but less agreement in the exact genes detected. Congruous with this, the HRV-HF screens showed a low percentage of exact gene overlap in the primary screen datasets (for DFs with $\leq$50% plate mean infected cells and $\geq$40% plate mean number of cells: Silencer Select 14.7%, esiRNA 17.6%, SMARTpool 14.7%, SMART-Rev 39.1%; Figure S1B, Table S2). A comparison across the screens for siRNAs targeting components of the V-ATPase, 80S ribosome, and elongation complex showed estimated false negative rates ranging from 10% to 40% (Table S2). We note that the only differences between the individual screen datasets in this effort are the siRNA libraries, demonstrating that library characteristics contribute to screen-to-screen variability. We generated a common candidate list for genes that scored in two or more of the three largest screens (Silencer Select, SMARTPool and esiRNA, common HRV-HFs; Figure S1B; Table S2). To minimize the effects of false positives/OTEs, we performed microarray analysis (Affymetrix GeneChip human 2.0 ST array) to determine the genes expressed in the H1-HeLa cells (Figure S1C; Table S3). The microarray probe-set values were matched to the genes present in the siRNA libraries: 17,070 (80.8%) and 17,168 (79.5%) genes with expression data in the SMARTpool and Silencer Select screens. The median of the negative control intron probe set served as a cutoff for gene expression, producing a list of 12,461 common genes in the siRNA libraries that are expressed in the H1-HeLa cells.

RIGER Analysis of the MORR HRV-HF Screens

In addition to OTEs, false negatives also occur frequently in RNAi screens (Adamson et al., 2012). This likely arises from variable reagent efficacy and toxicity and candidate selection with absolute thresholds. To mitigate this, we used the MORR screening strategy and adapted a published RNAi informatics program, RIGER, to quantitatively integrate all the datasets into ranked lists of either DFs (RIGER4-DF) or CFs (RIGER4-CF; Table S4) (Luo et al., 2008). The microarray gene-expression data was then used to identify HRV-HFs not expressed in the H1-HeLa cells as likely OTEs. We found that among the top 250 RIGER4 DF genes, 36 fell below the intronistic median (14.4%); these are noted on the candidate list with red fill because they are likely OTEs (Table S1).

We then compared the RIGER4 and primary dataset rankings from the individual screens for five test sets (80S Ribosome, V-ATPase, the elongation complex, MED, and the common 112 HRV-DFs). This was done by determining the area under the curve (AUC) produced by plotting the percentage of test genes from the total set that is detected moving from the top down along the respective gene rankings (Figures 1E and S1D; Table S4). The AUC analysis shows graphically how well an siRNA library or RIGER4 analysis detected the expected components. The AUC analyses show that the RIGER4 SB and WS methods performed better in the test cases and provided a

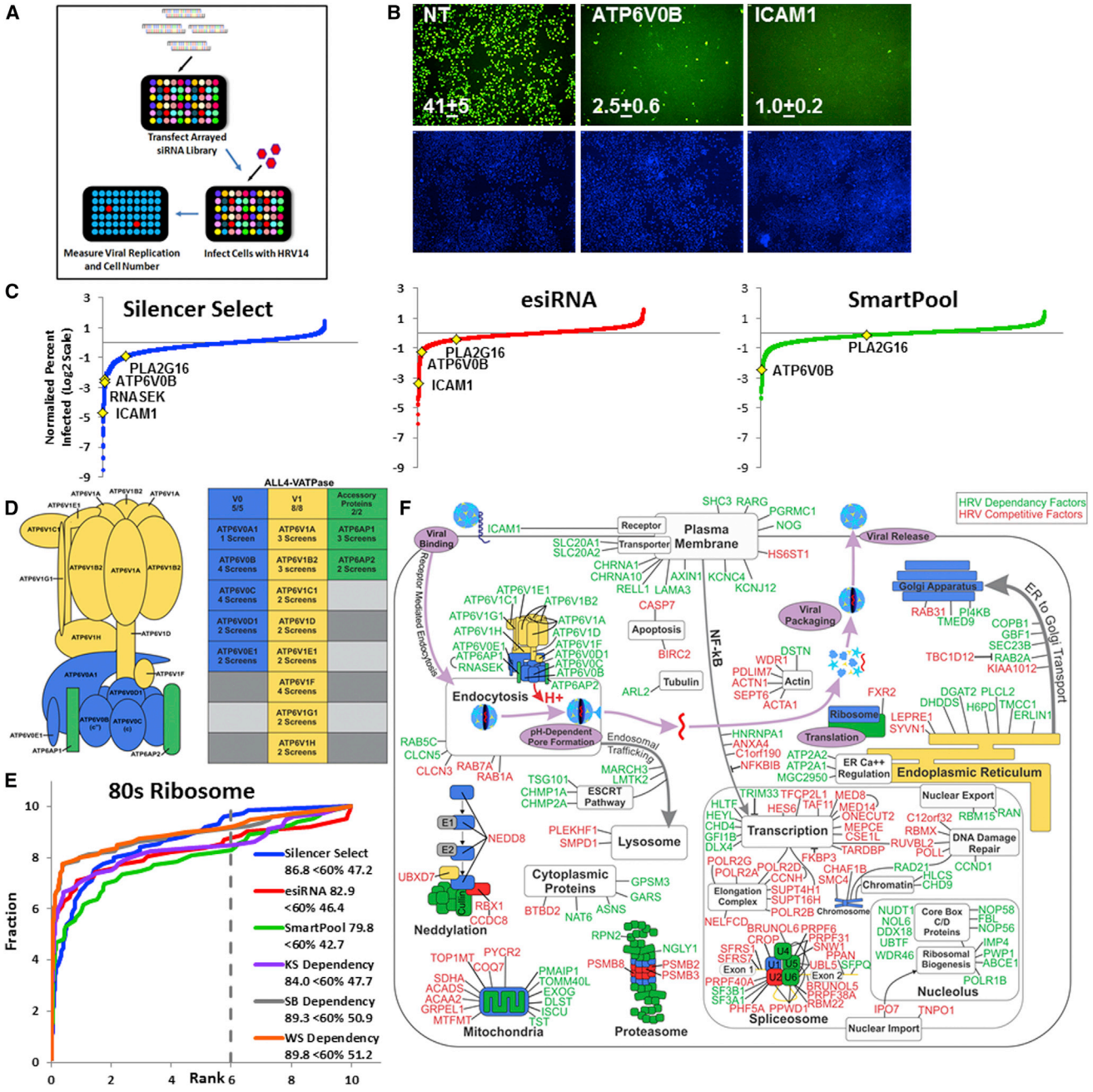


Figure 1. MORR Screens Identify Factors that Modulate HRV14 Replication

(A) Schematic of the HRV RNAi screen.

(B) H1-HeLa cells were transfected with the indicated negative (non-targeting [NT]) and positive (ATP6V0B, ICAM1) controls for 72 hr and then infected with HRV14 for 14 hr. Cells were then fixed, permeabilized, and immunostained with anti-HRV14 capsid antibody (green) or stained for DNA (blue). Percent infected cells ± SD are shown (×4).

(C) The results of the HRV screens with the siRNA pools ranked in order of their normalized percent infection (log2 scale). The highlighted genes are selected hits from that library.

(D) Schematic of the V-ATPase (left) (Marshansky et al., 2014), with components V_0 (blue), V_1 (yellow), and accessory proteins, including ATP6AP1 (green), that scored in one or more of the HRV screens (right).

(E) The RIGER4 analyses (weighted sum [WS], second best [SB], and Kolmogorov-Smirnov [KS]) and the individual MORR screen datasets were compared by assessing their respective levels of enrichment for components of the 80S ribosome. An enrichment score for each screen was calculated by determining the AUC

(legend continued on next page)

quantitative estimate for each gene's significance in HRV replication. Using the HRV lifecycle as a framework and with the referenced literature as a guide, 164 (96 DFs and 74 CFs) of the top 150 of both the DF and CF RIGER4 gene lists expressed in the HeLa cell were assembled into a schematic model (Figure 1F; Table S5). To make room, the ribosomal subunits were excluded. For 136 genes of the top 300 genes, there is insufficient existing literature to place them in the model. However, based on the enrichment of multiple complexes and pathways, we estimate that this model identifies the majority of HRV14's dependencies in HeLa cells.

RNASEK Is Required for the Replication of Multiple Viruses

Among the top HRV-DF candidates from the Silencer Select screen was RNASEK, a 137 amino acid dual-pass transmembrane protein with an undetermined cellular role, whose N- and C-termini are predicted to lie on the inside of the cell (Figure S1E) (Economopoulou et al., 2007; Kiritsi et al., 2012). RNASEK was not screened in the other three libraries and thus was not ranked by RIGER, demonstrating that RIGER analysis and a traditional validation approach are complementary. RNASEK is ubiquitously expressed and highly conserved across mammals, with 100% amino acid identity seen between mouse, rabbit, and human. RNASEK was previously listed in a siRNA screen candidate list as a gene required for CME, but was not evaluated further (Kozik et al., 2013). There are insect RNASEK homologs but no known yeast homolog.

RNASEK was needed for replication of HRV14, as well as IAV A/WSN/33 H1N1 (WSN/33) strain (Figures 2A, S2A, and S2B). To test the role of RNASEK in non-transformed cells, normal human fibroblasts were transduced with a lentivirus expressing either a short hairpin RNA (shRNA) against RNASEK or a scrambled control (shScr) and then infected with IAV WSN33 (Figure 2B). A rescue of HRV14 replication was done using cells stably transduced with a FLAG-tagged RNASEK (RNASEK-F) together with siRNAs directed against either the RNASEK coding sequence or the 3′ UTR (Figures 2C and 2D). RNASEK-F was used because available commercial anti-RNASEK antibodies did not perform well. We also attempted to express a RNASEK mutant reported to be inactive in vitro (Kiritsi et al., 2012); however, we were unable to express this mutant protein in HeLa cells. A validation method was used where the nucleotides at positions 9–11 on the antisense siRNA oligonucleotide are changed to the cognate bases (C9–11); this detects OTEs due to interactions with microRNA seed sequences (Buehler et al., 2012). Mutation of the C9–11 positions in either of two effective siRNAs targeting RNASEK resulted in enhanced viral infectivity together with decreased target depletion (Figures 2E–2G). Similar results were obtained using additional HRV serotypes, 1A and 16, which were selected because of their genetic divergence from HRV14 and one another (Figure S2C).

Cells depleted of either RNASEK or ATP6V0B were infected with either DENV2, 3, or 4, YF17D, the IAV strains, X31 H3N2, IAV WSN/33, or a pseudotyped Moloney leukemia virus (MLV) expressing the VSV-g fusion protein (Figures S2D–S2J). For each virus, depletion of either RNASEK or ATP6V0B lowered viral replication. No differences were seen when these same transfected cells were infected with either HIV-1-IIIB or MLV pseudotyped with the cytomegalovirus (CMV) envelope protein (Figures S2K and S2L).

RNASEK Is Needed for HRV and IAV Entry

The infectivity data suggested that RNASEK, like ATP6V0B, is required for viruses that enter cells via the endosomal pathway, but not for viruses that enter at the cell surface. To determine where in the viral lifecycle RNASEK is required, translocation assays were done wherein virus and siRNA-transfected cells were synchronously released from a chilled incubation state by the addition of warm media. Confocal images were obtained at the indicated time points (Figures 2H and 2I). These studies show that both HRV and IAV are predominantly blocked prior to entry into the cell when either RNASEK or ATP6V0B is depleted. When cells were treated with acidic buffer (pH 5), a portion of the IAV infection was rescued in either the RNASEK- or ATP6V0B-depleted cells, revealing that surface-bound IAV could undergo fusion with the host membrane (Figure S3A). The surface levels of ICAM1 were unchanged with RNASEK depletion (Figure S3B). In sum, these data show that HRV and IAV, and by extension DENV, YF17D, and VSV-g pseudoparticles, cannot effectively enter the cell when RNASEK levels are lowered.

RNASEK Closely Associates with the V-ATPase

To identify proteins that interact with RNASEK-F, affinity purification coupled to mass spectrometry (AP-MS) studies were done. These experiments identified multiple components of the V-ATPase, both V_0 and V_1 subunits, as well as clathrin heavy chain (CLTC), the clathrin adaptor, AP2, flotillin (FLOT1), and the transferrin receptor (TfR), as associating with RNASEK (Figures 2J and S3C; Table S6). Co-immunoprecipitation (co-Ip) experiments using anti-ATP6AP1 antibodies immunoprecipitated RNASEK-FLAG and did so after a high speed (100,000 × *g*) spin to clarify the lysate of membrane fragments (Figure S3D). In these experiments, the band containing RNASEK-F was seen to migrate below the immunoglobulin light chain protein at just above the 15 kDa size marker. ATP6AP1 (Ac45) is a type one transmembrane protein required for V-ATPase function that associates with the V_0 subunit (Jansen et al., 1998; Supek et al., 1994). ATP6AP1 also contains a C-terminal endocytic targeting signal that directs it from the cell surface into the endosomal pathway (Feng et al., 2008). Confocal imaging also showed that RNASEK-F partially colocalized with ATP6AP1 (Figure 2K).

generated by plotting the percent fraction (Fraction) of 80S component proteins encountered moving from the lowest to highest p value on the ranked gene lists (Rank). Numbers represent the percent enrichment of the total gene set at <60% of the ranked gene list.
(F) Based on the RIGER4 screen dataset, a hypothetical model cell was created highlighting the HRV lifecycle, as well as where 164 of the HRV-HFs might function based on available evidence (Table S5).

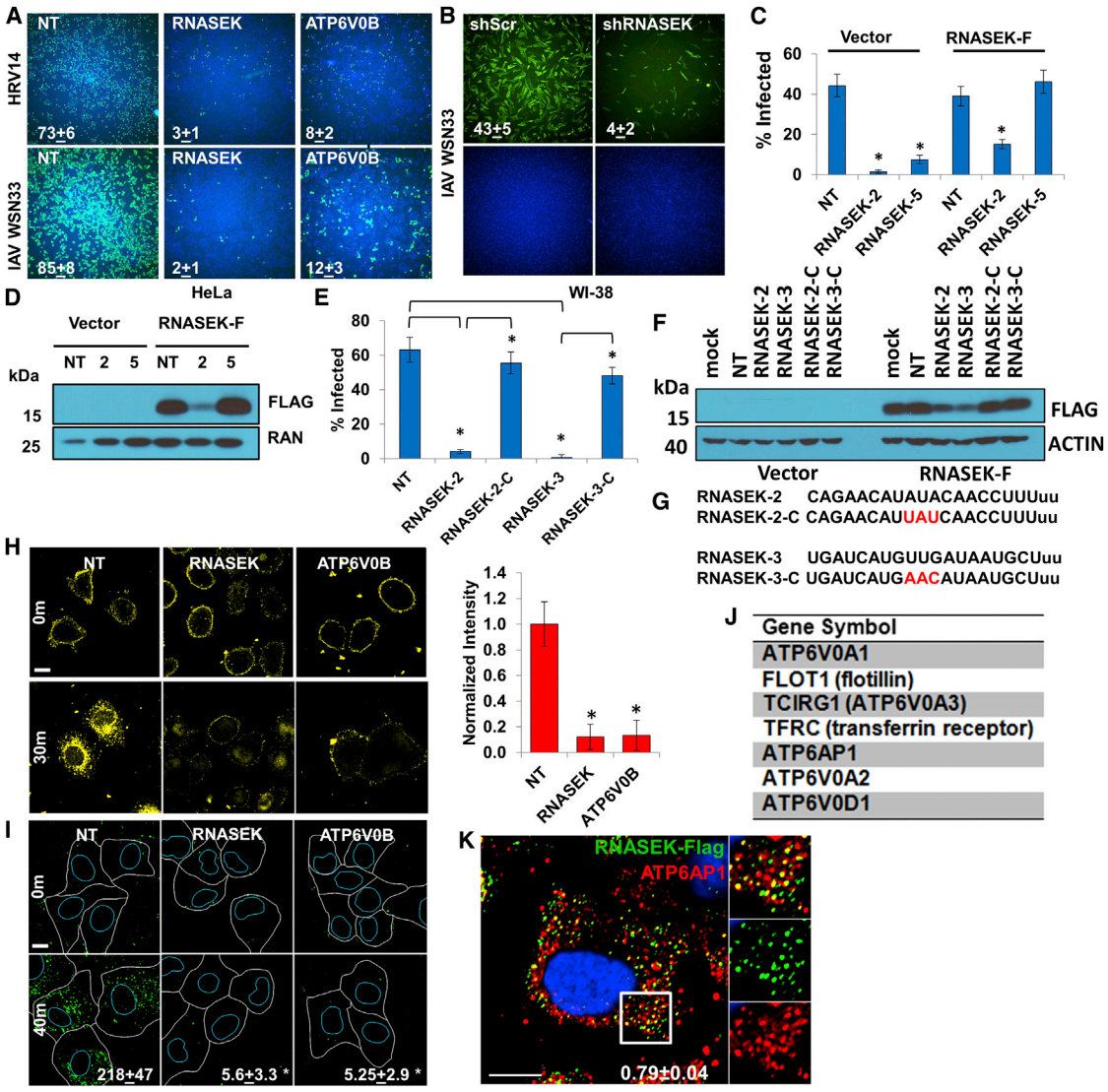


Figure 2. RNASEK Is Required for HRV and IAV Entry and Partially Associates with the V-ATPase

(A) H1-HeLa cells were transfected with the NT control siRNA or siRNAs targeting either RNASEK or ATP6V0B. Cells were infected with either HRV14 or IAV WSN33. Cells were stained for DNA (blue) and either an anti-HRV14 capsid antibody or an anti-HA antibody (green). The percentage of infected cells ± SD is shown (×4).

(B) Normal diploid human fibroblasts (WI-38 cells) were stably transduced with the indicated shRNA-expressing retroviruses. Cells were then infected with WSN33. After 14 hr, the cells were processed and analyzed as in (A).

(C) H1-HeLa cells stably transduced with retroviruses expressing either RNASEK-FLAG (RNASEK-F) or the empty vector control (Vector) were transfected with either a NT siRNA, a siRNA that targets the coding sequence of the RNASEK mRNA (RNASEK-2), or one against the 3′ UTR (RNASEK-5). At 72 hr after transfection, the cells were infected with HRV14 and processed as in (A).

(D) Whole-cell lysates from the cells in (C) were subjected to immunoblotting. RAN, loading control.

(E) RNASEK-F cells were transfected with the indicated siRNAs as well as their respectively matched C911 control siRNAs (-C). At 72 hr after transfection, the cells were infected with HRV14.

(F) Immunoblots of whole cell lysates from (E). Vector cells are shown for comparison. Actin, loading control.

(G) siRNA sequences used in the experiments in (E) and (F).

(H) H1-HeLa cells were first transfected with the indicated siRNAs for 72 hr and then incubated with HRV14 on ice. Warm media were added at time 0. Cells were fixed at the indicated time points, stained with anti-HRV14 antibody (yellow), and confocally imaged. Quantitation of viral entry is provided at right (normalized mean intensity ± SD) for ≥15 cells from each of n = 3 experiments (×63). Scale bar represents 10 μM.

(I) As in (H), but cells were incubated with IAV A/Puerto Rico/8/34 H1N1 (PR8) and stained with anti-NP antibody (green). Nuclei are outlined in blue and the cell peripheries in white.

(J) Proteins interacting with RNASEK-F using AP-MS. Proteins shown were identified from multiple peptides in two or more experiments (Table S6).

(legend continued on next page)

RNASEK Is Needed for Endocytosis

RNASEK associates and co-localizes with the V-ATPase, FLOT1, and TfR and is required for the entry of HRV and IAV and is highly conserved across species. We tested whether RNASEK was needed for the endocytosis of transferrin, high molecular weight (hmw) dextran, or cholera B toxin (CTb). The depletion of RNASEK inhibited the entry of transferrin via clathrin-mediated endocytosis (CME), similar to what was observed with targeting ATP6V0B (Figure 3A) (Kozik et al., 2013). The silencing of either RNASEK or ATP6V0B also decreased the entry of dextran by macropinocytosis (Figure 3B). However, only the loss of RNASEK decreased the entry of CTb, suggesting that non-CME was the predominant mode of CTb entry in this setting (Figures 3C and S3E; Supplemental Information). Therefore, while the loss of either RNASEK or ATP6V0B produced comparable effects with both transferrin and dextran, only RNASEK depletion inhibited the endocytosis of CTb, demonstrating that these factors have both similar and unique functional roles.

Loss of RNASEK or the V-ATPase Increases Endo-lysosomal Acidity

Reducing endosomal acidity inhibits HRV entry (Fuchs and Blaas, 2012). RNASEK interacts with the acidifying complex, V-ATPase. We depleted RNASEK and looked for an effect on endo-lysosomal acidity using acidophilic dyes: Lysotracker red (LTRed), Lysotracker green 26 (LTG-26), or Lysosensor green 153 (LSG-153). We used the LSG-153 dye because its signal increases with increasing acidity, while LTRed becomes fluorescent at a threshold and does not thereafter increase with decreasing pH. Surprisingly, lowering the levels of either RNASEK or ATP6V0B resulted in increased intracellular acidity, which was sensitive to the small molecule, bafilomycin A1 (BAF; Figures 4A and S4A); this phenotype was rescued in the setting of a siRNA-resistant RNASEK-F (Figure S4B). Similar results were obtained using normal fibroblasts transduced with shRNASEK (Figures 4B and 4C). Reducing RNASEK levels, or those of two V-ATPase subunits, in RAB7-GFP-expressing or RAB7-red fluorescent protein (RFP)-expressing cells, expanded the RAB7 compartment, which co-localized with the acidic dye signal (Figures 4D–4F). A subunit, ATP13A2, of an additional BAF-sensitive acidifying complex, the P-ATPase, co-localized with the LTRed signal seen with RNASEK or ATP6V0B depletion (Figure 5A) (Dehay et al., 2012b). shRNA-mediated depletion of ATP13A2 also increased intracellular acidity, as shown previously (Dehay et al., 2012b). However, decreasing the levels of either RNASEK or ATP6V0B together with ATP13A2 did not increase late endosomal acidity and also prevented the increased acidity seen after addition of Torin, a small molecule that induces autophagy and endo-lysosomal acidity (Figures 5B and S4C). This result shows that the loss of both the V-ATPase and the P-ATPase prevents the increased acidity observed with the induction of autophagy by Torin. Unlike what we observed with RNASEK or the V-ATPase, diminishment of ATP13A2 alone did not decrease HRV infection (Figure S4D). These data show that while the V-ATPase and P-ATPase are functionally redundant for late endosomal and lysosomal acidification the V-ATPase and RNASEK are uniquely required for viral entry and infection.

RNASEK Depletion Produces Enlarged CCPs

V-ATPase depletion or BAF treatment has been shown to produce enlarged CCPs in the setting of a block to CME, possibly due to a mislocalization of cholesterol (Kozik et al., 2013). The effect of RNASEK depletion on CCPs and cholesterol was evaluated using confocal imaging of cells immunostained for the CCP adaptor protein, CALM. As seen in previous studies (Kozik et al., 2013), lowering the levels of a V-ATPase subunit produced enlarged CCPs (Figure 5C); these data also show that decreasing RNASEK levels increased both the staining intensity and the number of CALM-containing CCPs; this phenotype was rescued by the expression of a siRNA-resistant RNASEK-F transgene (Figures S4E and S4F). However, no alteration in cholesterol distribution was seen in cells depleted of RNASEK or any of several V-ATPase components, and the addition of exogenous cholesterol did not rescue the block to transferrin entry seen under these conditions (Figures S5A–S5C). Indeed, exogenous cholesterol decreased transferrin uptake. The addition of the proton ionophore, Nigericin, rapidly reduced acidity (<10 min), increased CALM staining, and inhibited transferrin entry as expected and did so without altering the distribution of cholesterol (Figures S5D–S5F). Imaging of the adherent cell surface revealed that either RNASEK or ATP6V0B depletion resulted in a portion of the cell-associated endocytic cargo (HRV14 or transferrin) being trapped within enlarged CCPs (Figures 5D–5F). Consistent with the increased CALM signal observed with RNASEK or ATP6V0B depletion, we also observed an increase in the number and depth of CCPs at a point prior to scission (tethered CCPs) using transmission electron microscopy (TEM; Figures 5G–5I). Similar results were obtained using super-resolution microscopy (Deltavision Localization Microscopy [DLM] system), with both the intensity and size of CALM- and CLTC-containing CCPs increasing with either RNASEK or ATPV0B depletion (Figures 6A–6D, S5G, and S5H).

RNASEK Modulates CCP-Associated V-ATPase Location and Levels

CCPs form via the sequential assembly of multiple factors (Figure 7A) (Kirchhausen et al., 2014). An endocytic signal, i.e., a ligand binding to its receptor, triggers the membrane association of FCHo1/2 and the adaptor proteins, EPS15, AP2, and CALM, which bind to one another and recruit clathrin, which surrounds the developing CCP. DNM2 is then recruited and mediates scission and vesicle formation. To investigate the enlarged CCPs occurring with either RNASEK or V-ATPase depletion, we evaluated for the above factors, as well as for RNASEK, ATP6AP1, and ATP6V0B. Confocal imaging of the cell membrane-coverslip interface, as well the middle of the cell, showed that loss of RNASEK decreased the signals of three V-ATPase subunits

(K) RNASEK-F cells were immunostained with the indicated antibodies. The fraction of colocalization of RNASEK-Flag (green) with ATP6AP1 (red) ± SD averaged across n = 4 independent experiments is provided; ≥ 15 cells per condition per experiment were evaluated. The value represents the Mander's coefficient for the flag channel and therefore is the percent of RNASEK-Flag that is colocalized with ATP6AP1.
Scale bar represents 10 μM. ×63. Results throughout are the mean of n ≥ 3 independent experiments ± SD. *p ≤ 0.05 (Student's t test).

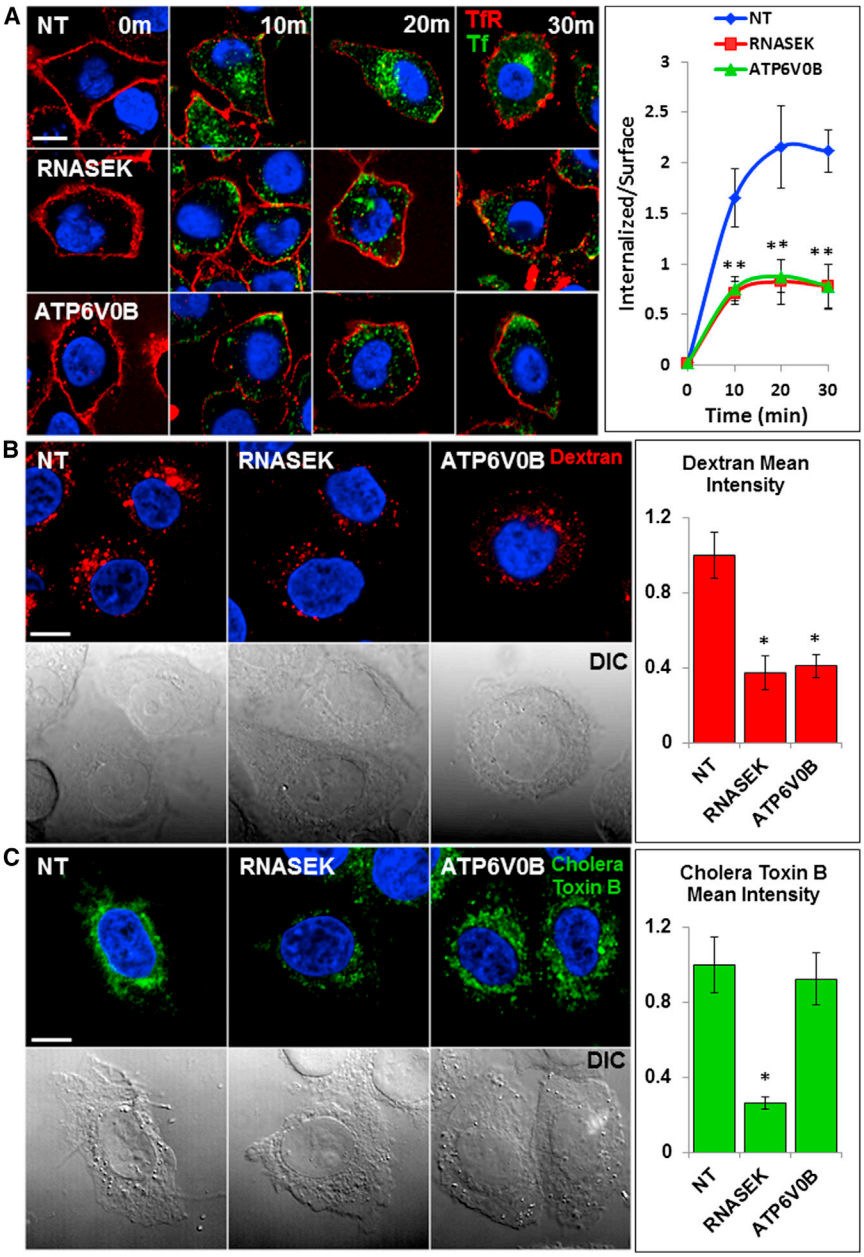


Figure 3. RNASEK Is Required for Endocytosis

(A) H1-HeLa cells were transfected with the indicated siRNAs and then incubated with transferrin-FITC (green). At the indicated time points, cells were washed with stripping buffer, fixed, stained for transferrin receptor (TfR, red), then confocally imaged. The ratios of internalized transferrin to surface TfR at the indicated times are at the right. Nuclear DNA (blue).

(B) As in (A), but cells were incubated with high molecular weight Dextran conjugated to Alexaflour 586 (red) for 20 min prior to a brief trypsin treatment and fixation.

(C) As in (A), but cells were incubated with Cholera toxin B-FITC (green) for 20 min prior to a brief trypsin treatment and fixation.

Results throughout are the mean n = 3 experiments ± SD. DIC images are shown below. ×63; scale bar represents 10 μM. Results throughout are the mean of ≥15 cells per condition from three independent experiments ± SD. *p ≤ 0.05 (Student's t test).

(ATP6AP1, ATPV0D1, and ATP6V0B), similar to what was seen with loss of ATP6V0B (Figures 7B, S6A, and S6B).

While CCPs are smaller (60–100 nM) than the limits of resolution of confocal microscopy (>250 nM), we reasoned that immunofluorescence (IF) signals would nonetheless be proportional to the changes seen with TEM and super-resolution microscopy. Furthermore, using IF we could efficiently characterize the relative levels of CCP-associated proteins using a panel of antibodies. Therefore, we created 3D reconstructions of confocal images of the CCPs projecting into the cell from the cell membrane-coverslip interface. Consistent with published work on the V-ATPase (Kozik et al., 2013), an increase in CCP size was seen at the bottom surface (attached to the coverslip) of the cells when either RNASEK or ATP6AP1 were diminished (Figures 7C, 7D, S6C, and S6D). Similar results were obtained when we imaged the top surface of these cells (Figures S6E and S6F). A comparison of the relative size of the structures seen with the TEM (CCPs) and confocal images (CALM signals; Figure S6G) shows that the relative differences in the CALM signals seen in the confocal IF images are in keeping with the relative differences seen with the CCPs with TEM. While the confocal images need to be interpreted with their limited resolution in mind, they nonetheless permitted us to look at the relative presence of multiple CCP-associated proteins using immunostaining. The confocal images also showed that both RNASEK and ATP6AP1 are present just below the membrane surface with many of their signals originating near the inner membrane at the base of the CCPs (Feng et al., 2008; Jansen et al., 2012). Moreover, 58% ± 10% of RNASEK and 46% ± 14% of ATP6AP1 colocalize with the corresponding factor, and >40% of each of these proteins colocalized with CALM, with colocalization defined as the percentage of directly overlapping pixels (Figures 7C, 7D, and S6H). The image analysis software used does not permit blending of colocalized signals in the merged 3D images, resulting in one of the two signal channels shrouding the other.

Depletion of RNASEK reduced the size of the ATP6AP1 signal, and the converse was also seen; however, while the reduced RNASEK signal remained at the CCP's base, the remaining ATP6AP1 moved away from the inner membrane leaflet and further up the associated CCP (Figure 7E). Similar results were

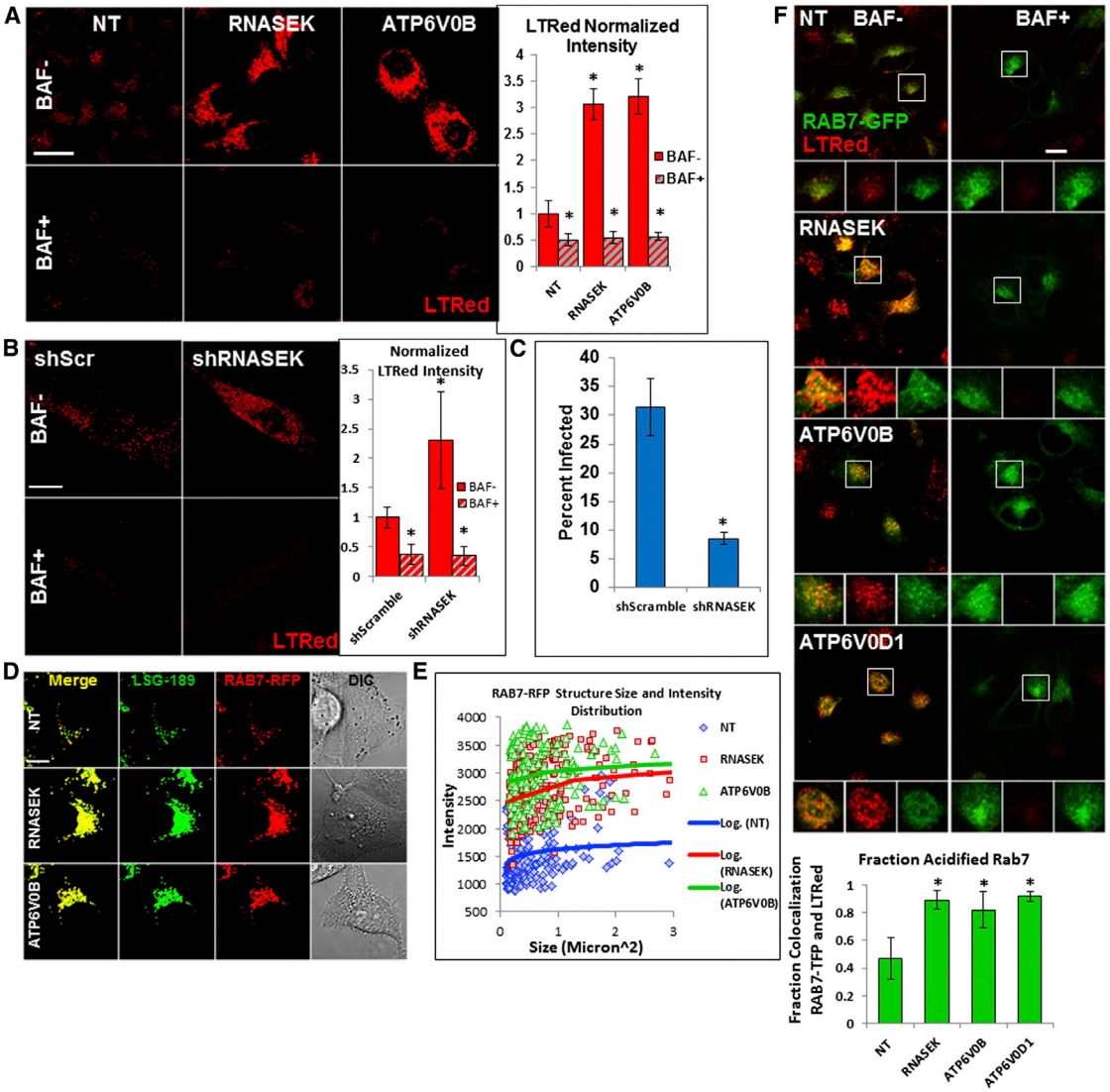


Figure 4. Depletion of Either RNASEK or the V-ATPase Increases Endo-lysosomal Size and Acidity

(A) H1-HeLa cells were transfected with the indicated siRNAs then incubated with lysotracker red (LTRed) in the presence or absence of bafilomycin A1 (BAF).

(B) Normal diploid human fibroblasts (WI-38 cells) were stably transduced with the indicated shRNAs and incubated with LTRed.

(C) Cells in (B) were infected with IAV WSN33 then stained with anti-HA.

(D) H1-HeLa cells stably transduced with RAB7-RFP (red) were transfected with the indicated siRNAs and then incubated with Lysosensor green 189 (LSG-189, green), and the cells were imaged live.

(E) Quantitation of the size or acidity (intensity) of the RAB7-RFP-containing late endosomes and lysosomes from cells in (D). ×63; scale bar represents 10 μM.

(F) H1-HeLa cells stably transduced with a RAB7-GFP (green) lentivirus were transfected with the indicated siRNAs then incubated with LTRed and confocally imaged. The fraction of RAB7-GFP colocalizing with LTRed ± SD from multiple cells in from multiple fields is shown graphically below. ×63; scale bars represent 10 μM. Results throughout are the mean of ≥15 cells per condition from n = 3 experiments ± SD. *p ≤ 0.05 (Student's t test).

seen with ATP6V0B (Figures 7F and S7A). These data suggest that both RNASEK and ATP6AP1 reciprocally regulate the others' levels and distribution at the plasma membrane, with RNASEK also being needed to position ATP6AP1 or ATP6V0B at the base of the CCP. Immunoblots of lysates from separate aliquots of these same cells revealed that loss of RNASEK or ATP6V0B decreased the total cellular levels of ATP6AP1 and to a lesser extent ATPV0D1, but not ATPV0A1, showing that RNASEK is necessary for maintaining cell wide levels of ATP6AP1 (Figure 7G).

Loss of ATP6AP1 was found to strongly inhibit HRV replication in the screens as well as in follow-up assays (Figure 7H; Table S1). Depletion of cholesterol, as determined by lower Filipin staining, decreased the magnitude of the CALM signals (Figure S7B). The reduced magnitude of the CALM signals with loss of cholesterol is consistent with studies showing that lower cholesterol caused flattening of CCPs as viewed by TEM (Subtil et al., 1999), arguing against low cholesterol being the cause of the enlarged CCPs seen with the loss of V-ATPase or RNASEK (Kozik et al., 2013).

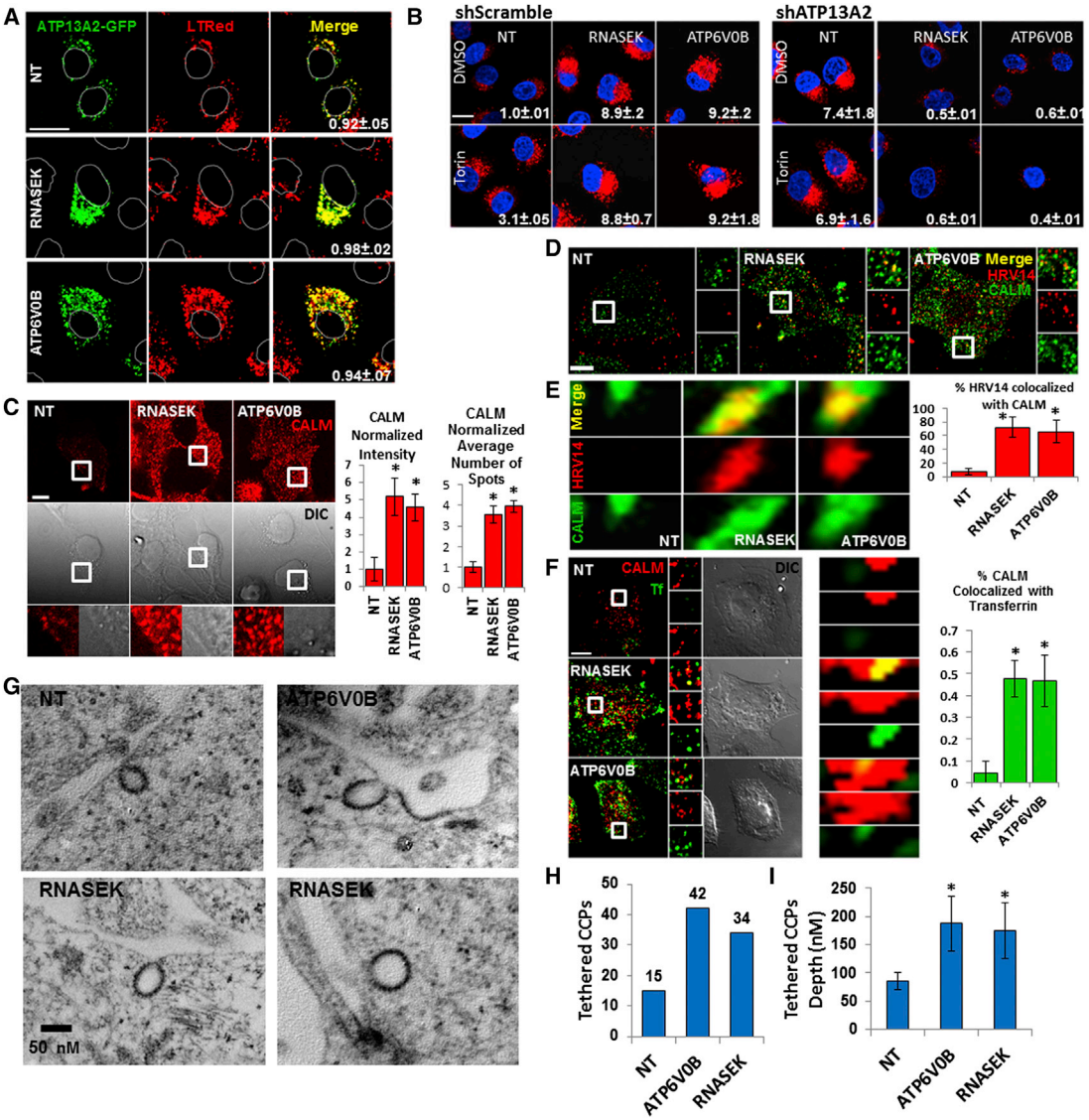


Figure 5. The V-ATPase and P-ATPase Function Redundantly to Regulate Endo-lysosomal Acidity and Depletion of RNASEK Enlarges CCPs

(A) H1-HeLa cells were stably transduced with ATP13A2-GFP, transfected with the indicated siRNAs, and then incubated with LTRed and confocally imaged. Numbers represent the fraction of ATP13A2-GFP colocalizing with LTRed ± SD. ×63; scale bar represents 10 μM.

(B) H1-HeLa cells stably transduced with lentiviruses expressing either a negative control (shScramble) or one against ATP13A2 (shATP13A2) were transfected with the indicated siRNAs. Cells were then treated with either Torin or the DMSO control for 3 hr and then incubated with LTRed. ×63; scale bar represents 10 μM.

(C) H1-HeLa cells transfected with the indicated siRNAs then stained for CALM (red) and confocally imaged at the interface of the cell membrane and glass coverslip (bottom surface). ×63; scale bar represents 10 μM. Quantitation is at the right.

(D) As in (C), but cells were incubated with HRV14 on ice. Warm media were added, and cells were then fixed and immunostained with anti-HRV14 antibody (red) and anti-CALM antibody (green) and then confocally imaged.

(E) Confocal images of cells in (D) at the cell interface with the glass coverslip. The CALM-containing CCPs (green) are shown extending from the inner cell membrane leaflet (top of the image) into the cytosol. The depth of each stacked image is 2 μm.

(F) H1-HeLa cells were transfected with the indicated siRNAs then incubated with transferrin-FITC (green). Cells were then immunostained for CALM (red) and confocally imaged at the interface of the cell and glass coverslip. The column of matching images at the right shows representative CALM-containing CCPs (red) that are extending from the cell membrane (top) into the cytosol. Quantitation is at the right.

(G) H1-HeLa cells were transfected with the indicated siRNAs and then processed and imaged using TEM. Representative electron micrographs of the membrane-associated tethered CCPs are shown for each condition.

(H) Quantification of the tethered CCPs (connected to the plasma membrane) seen in cells in (G). The values are the number of tethered CCPs from 50 cells evaluated for each condition, n = 3 independent experiments.

(I) Measurement of the tethered CCPs' depth (long axis from the plasma membrane to the base of the CCP). The values are the depth in nM (average ± SD) of the tethered CCPs from (H).

Images are representative of N = 3 independent experiments. *p ≤ 0.05 (Student's t test).

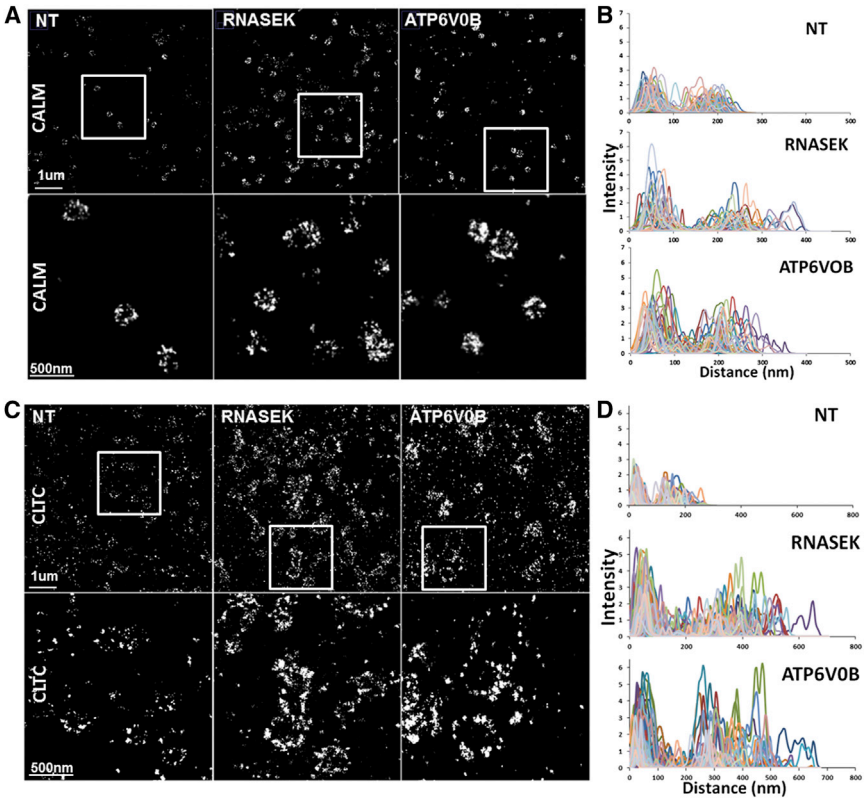


Figure 6. Super-Resolution Imaging of CCPs with RNASEK or ATPV0B Depletion

(A) DLM super-resolution microscopy images showing CALM staining at the adherent surface of HeLa cells transfected with the indicated siRNAs. Top row shows a representative field and the bottom row shows a zoomed area (white box).

(B) Intensity profiles from the DLM super-resolution images of 60 individual CCPs identified by CALM immunostaining for each of the indicated conditions. These results are representative of a total of 120 individual CCPs analyzed across three independent experiments.

(C) DLM super-resolution images showing clathrin heavy chain (CLTC) immunostaining as in (A).

(D) Intensity profiles from the DLM super-resolution imaging of 68 individual CCPs identified by CLTC staining for each of the indicated siRNA-transfection conditions. These results are representative of a total of 138 individual CCPs analyzed across three independent experiments.

Additional parameters are in the Supplemental Information.

We further characterized the CCPs. Depletion of RNASEK or ATP6V0B did not alter the relative levels of CCP-associated EPS15 or AP2 (Figures S7C and S7D). As expected, CLTC strongly co-localized with CALM (Figure S7E). Finally, we immunostained for DNM2 and detected equivalent levels present at the CCP after RNASEK or ATP6V0B depletion (Figures S7F and S7G). Therefore, these studies indicate that RNASEK regulates the levels of the V-ATPase at the cell membrane and in the endosomal pathway and suggest that RNASEK is required for V-ATPase function, the loss of which decreases endocytosis.

DISCUSSION

To obtain a systems level view of HRV's host factor dependencies, we undertook parallel genetic screens using MORR. We chose to use MORR to take advantage of the best that each of the large-scale RNAi resources has to offer and to offset the caveats of RNAi screening. The HRV-HF candidates from the primary screens were further evaluated using both traditional validation and phenotypic quantitation with RIGER to minimize false positives and false negatives. This effort identified both known and previously unappreciated HRV-HFs. A published *Drosophila* screen using a picornavirus reported 65 ribosomal subunits that were needed for viral replication; a comparison showed that depletion of the human homologs of 55 of these genes lowered infectivity in one or more of the screens (Table S7) (Cherry et al., 2005). Apart from the ribosome, an additional 16 of 38 (42%) of the corresponding human homologs from the *Drosophila*-based screen also scored in one or more of our screens; this comparison suggests that high-confidence candidates that are unique to the MORR screens also play roles in HRV replication, revealing the need for screens using human cells and pathogens. The top candidates in this quantitatively integrated HRV-HF dataset likely represent the majority of the factors needed by HRV in vitro, thus providing a comprehensive resource for picornavirus research (Figure 1F).

From among the HRV-HFs, we further investigated RNASEK, whose loss inhibited multiple HRV serotypes, IAV and DENV. Decreasing the levels of RNASEK resulted in (1) halting viral infection at the cell surface, (2) a decrease in CME and non-CME, and (3) the appearance of enlarged CCPs. RNASEK was detected in CCPs and immunostaining of an exogenously expressed RNASEK-F protein demonstrated an endosomal pattern. Proteomics revealed that RNASEK associated with multiple V-ATPase proteins. RNASEK also associated with components of CCPs (Table S5); this is in line with confocal images of both RNASEK and ATP6AP1 partially colocalizing with one another and with CCPs at the cell membrane.

Many of the phenotypes seen with loss of RNASEK resemble those seen with V-ATPase depletion. Confocal imaging showed that RNASEK was necessary to maintain the levels of some V-ATPase components at both the cell membrane and the cell interior; a closer evaluation also revealed that these V-ATPase components moved away from the cell surface to a more distal portion of the CCP. In the case of ATP6AP1, loss of RNASEK also resulted in lower cellular levels. In turn, lowering ATP6AP1 levels also decreased the levels of RNASEK. These data demonstrate that RNASEK interacts with ATP6AP1 and that they reciprocally control each other's levels at the cell

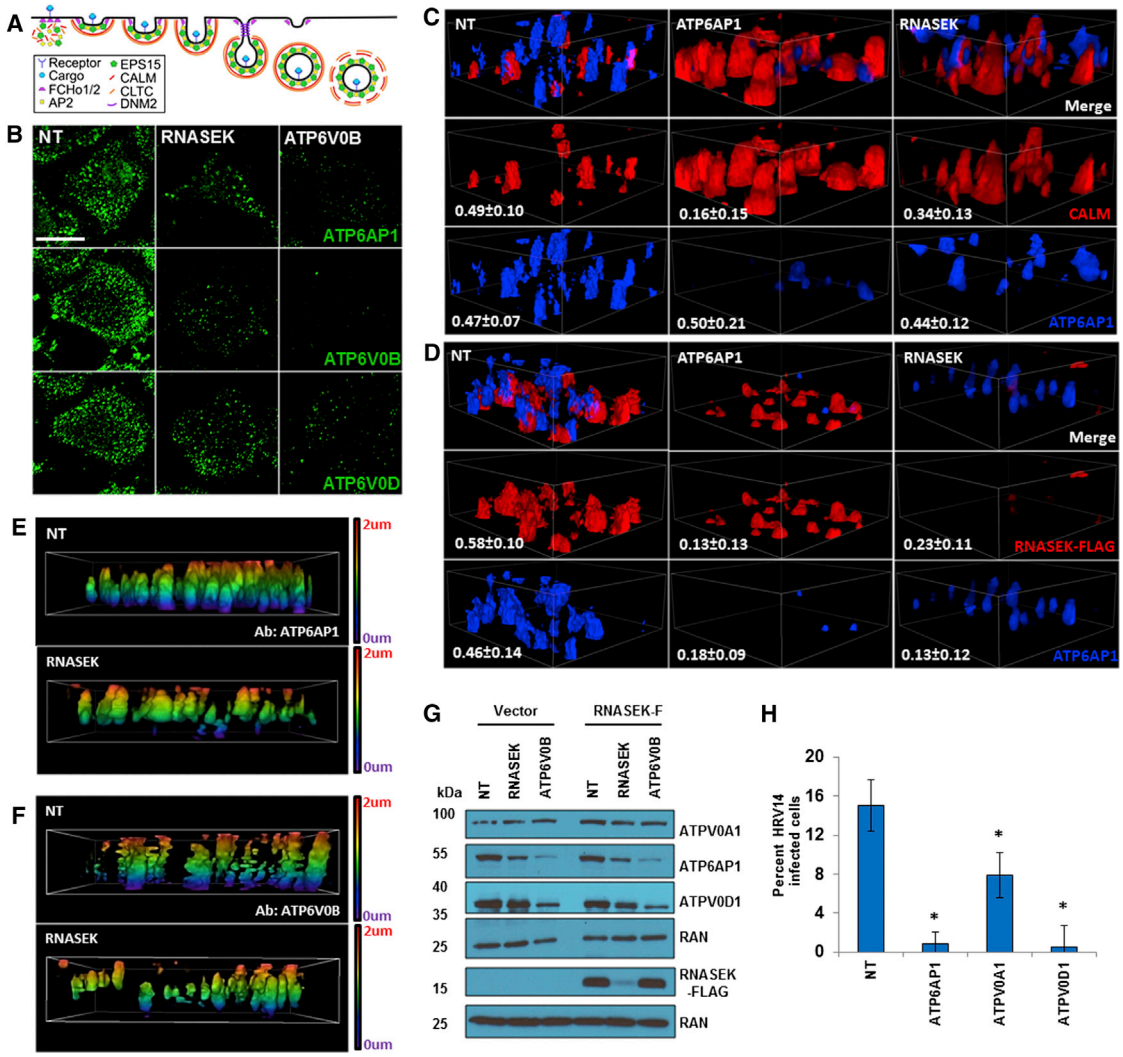


Figure 7. RNASEK Is Needed for V-ATPase Function and Characterization of the RNASEK- or V-ATPase Depletion-Induced CCPs

(A) Schematic model depicting the assembly of factors that form a CCP and direct its evolution into a CCV.

(B) H1-HeLa cells were transfected with NT, RNASEK, or ATP6V0B siRNAs (top of each column in white) and then stained with the indicated antibodies (green) and confocally imaged at the interface between the cell and the coverslip. ×63; scale bar represents 10 μM. Quantification is shown in Figure S6B (bottom slice).

(C and D) RNASEK-F cells were transfected with the indicated siRNAs (top left of each column) and then stained with the indicated antibodies (bottom right of each row). 3D reconstructions were created of confocal images progressing from the cell-coverslip interface to a height of ~2 microns. The dimensions of the white box are 6 × 6 × 2 μM. The fractions of colocalization are shown ± SD, with colocalization defined as the fraction of directly overlapping pixels. This software does not permit blending of colocalized signals in the merged images, resulting in one of the two signal channels shrouding the other. Images are representative of n = 3 independent experiments.

(E and F) H1-HeLa cells were transfected with the indicated siRNAs (top left) and then stained with the indicated antibodies (bottom right). 3D reconstructions were created of confocal images as in (C). Imaging software was used to colorize the resultant structures in a graded manner commensurate with elevation above the cell-coverslip interface with purple at the bottom and red at the top as represented by a bar showing a heat map at the right of each panel.

(G) RNASEK-F or vector cells were transfected with the indicated siRNAs. Cell lysates were probed with the indicated antibodies.

(H) H1-HeLa cells were transfected with siRNAs directed against the V-ATPase subunits shown or a NT control. The cells were then infected with HRV14. Results throughout are the mean of n = 3 experiments ± SD. *p ≤ 0.05 (Student's t test).

membrane and cell interior. A similar relationship was seen between RNASEK and ATP6V0B. In contrast, loss of these factors increased the RAB7 compartment, arguing that their loss does not simply dissipate the detectable levels of all endosomal proteins. We conclude that RNASEK is required for the correct localization and cellular levels of certain V-ATPase subunits, explaining its important role in endocytosis and viral replication.

We found that RNASEK is needed for both CME and clathrin-independent endocytosis; this is one difference observed between depletion of the V-ATPase components and RNASEK and as such suggests that RNASEK may act upstream of a

Table 1. Antibodies for Immunoblotting Experiments

Primary Antibody	Supplier (Catalog No.)	Dilutions
FLAG M2	Sigma (F1804)	WB (1:1,000)
β-Actin	Sigma (A2228)	WB (1:5,000)
RAN	Sigma (R4777)	WB (1:2,000)
ATP6V0A1	Sigma (AV46581)	WB (1:1,000)
ATP6AP1	Abcam (176609)	WB (1:200)
ATP6V0D1	Abnova (H00009114-M01)	WB (1:1,000)

Secondary antibodies are as follows: anti-rabbit horseradish peroxidase (HRP)-conjugated antibody (catalog number 111-035-003; Jackson ImmunoResearch) WB (1:10,000) and anti-mouse horseradish peroxidase (HRP)-conjugated antibody (catalog number 115-035-003; Jackson ImmunoResearch) WB (1:10,000). WB, western blot.

common membrane scission event or alternatively may somehow alter the environment at or adjacent to the plasma membrane. IAV is also thought to enter cells via redundant CME and non-CME mechanisms; therefore, the need for RNASEK in IAV entry is in keeping with these data. DNM2 is required for CME and caveloae-mediated endocytosis. We saw that with RNASEK depletion DNM2 was present at relatively the same levels at the CCPs, suggesting that its actions after arrival are somehow reduced with loss of RNASEK.

Surprisingly, decreasing RNASEK or V-ATPase levels increased both the acidity and size of the RAB7-containing compartment. In spite of this level of acidification, endocytosis and HRV replication were inhibited. Loss of the P-ATPase, together with either RNASEK or ATP6V0B, decreased basal and autophagy-related acidification. Therefore, the two ATPases and RNASEK are functionally redundant for acidification of the endo-lysosomal compartment. However, why all three must be present to correctly modulate the size and acidity of endo-lysosomes remains to be determined. In respect to endocytosis, including the progression of CCPs to endosomes, RNASEK and the V-ATPase possess non-redundant roles with the P-ATPase, revealing that the critical task of forming and acidifying nascent endosomes depends on both factors.

The enlarged CCPs seen in the setting of RNASEK or V-ATPase loss possessed DNM2. Together with the lack of viral entry and the endocytic cargo detected in the enlarged CCPs, these data reveal that the enlarged CCPs are somehow hindered in undergoing scission to become CCVs. This is consistent with our TEM and super-resolution microscopy data, which showed an increase in the number and size of CCPs that were associated with the plasma membrane. Loss of RNASEK also resulted in decreased CCP-associated ATP6AP1 and ATP6V0B, in addition to the migration of these factors away the CCP-membrane junction. Why does the loss of RNASEK or the V-ATPase block endocytosis and perturb CCPs? Possible mechanisms may involve RNASEK and V-ATPase interacting with additional components to aid DNM2 in endosomal scission. A precedent for this is seen in *Drosophila* retina development, where the proteolipid V_0 portion of the V-ATPase interacts with SNAREs to facilitate synaptic vesicle exocytosis (Hiesinger et al., 2005). However, one issue with this scenario is that the V-ATPase components were not detected in all of the CCPs, and one cannot rule out that RNASEK and the V-ATPase subunits are not simply trafficking along the endocytic pathway toward their definitive destination. This last possibility suggests a more downstream role for RNASEK and the V-ATPase, one in which they generate a proton gradient and perhaps also act as pH sensors to stimulate CCV generation and endocytic flux (Marshansky, 2007). Support for this notion comes from the production of enlarged CCPs seen shortly after addition of the proton ionophore Nigericin. Additional studies are needed to address these possibilities and to elucidate the mechanism by which RNASEK and the V-ATPase control the early events of endocytosis and viral replication.

EXPERIMENTAL PROCEDURES

Cell Lines

HeLa H1 cells (#CRL-1958) and WI-38 cells were from ATCC (#CCL-75). HeLa T4 cells were from NIH AIDS Reagent Repository. Cells were cultured in DMEM (Sigma) with 5% fetal bovine serum (GIBCO).

Viruses

HRV1A and HRV14 were from ATCC. The HIV-1 IIIB strain is from the NIH AIDS Repository. DENV serotype 2 New Guinea C is from ATCC. DENV serotypes 3 and 4 are primary isolates from Thailand and were kind gifts from Dr. G.C. Perng (Tainan University). Pseudotyped viruses were created by co-transfecting pCG-VSV-g or a plasmid expressing the CMV envelope together with pCG-Gag-Pol and MLV-GFP. IAV A/WSN/33 (WSN/33, H1N1 a kind gift of Dr. Peter Palese, Mount Sinai School of Medicine), A/Puerto Rico/8/34 H1N1 (PR8), and A/Aichi/68 (H3N2, X31, Charles River Labs) were propagated and tittered as previously described (Brass et al., 2009). IAV-infected cells were fixed 14 hr after infection using 4% paraformaldehyde (PFA, Sigma) in Dulbecco's PBS (D-PBS, Invitrogen). IAV-infected cells were immunostained for HA expression using either an anti-HA monoclonal (WSN/33 Wistar Institute; John et al., 2013) or anti-NP antibodies (H3N2, Millipore clone H16-L10-4R5 anti-IAV virus antibody). Pseudoparticles were produced using the noted envelopes as previously described (Feeley et al., 2011).

Antibodies

For the screens, we used the primary antibody anti-HRV14 V1 capsid antibody mab17 (kind gift of M.A. Poritz) and the secondary antibody goat anti-mouse Alex-Flour 488 (Invitrogen).

Immunoblotting

Cell lysates were made with Laemmli buffer and resolved by SDS/PAGE, then transferred to Immobilon-P membrane (Millipore), and probed with the indicated antibodies in Table 1.

Plasmids

pQCXIP-RNASEK-FLAG (RNASEK-F) was constructed using the pQCXIP retroviral vector (Clontech) and AgeI and BamHI sites, translation without FLAG tag (which is on the C terminus): MASLLCCGPKLAACGIVLSAWGVIM LIMLGIFFNVHSAVLIEDVPFTEKDFENGPQNIYNLYEQVSYNCFIAAGLYLLLG GFSFCQVRLNKRKEYMVR, transcript Refseq: NM_001004333.4. The human RAB7-GFP and -RFP constructs were made by cloning the cDNA in frame with the respective fluorescent protein at the C terminus and expressed from the lentiviral vector pLVX-puromycin (Clontech), which contains a puromycin resistance cassette. pLKO.5 shRNASEK was designed using the siRNA sequence for RNASEK from the Silencer Select siRNA library with a modified mir25 loop; the sequences for the oligonucleotides are 5′-CCGGTAGAACAT ATACAACCTTTACCTCTCAACACGGTAAAGGTTGTATATGTTCTTTTTTTG-3′ and 5′-AATTCAAAAAAAGAACATATACAACCTTTACCGTGTTGAGAGGTAAA GGTTGTATATGTTCTA-3′.

The oligo nucleotides were annealed then cloned into pLKO.5 (pLKO_TRC005; The RNAi Consortium) after digestion with AgeI and EcoRI restriction enzymes. Pseudotyped viruses were produced using pCG-VSV-g and ps.PAX2 vectors. pEGFP-N1 ATP13A2 (kanamycin resistant) and pLKO.1 shATP13A2 (sh403, 5′-CCGGGCCCATCAACTTCAAGTTCTAGTCGAGTAGA ACTTGAAGTTGATGGGCTTTTTG-3′) were the kind gifts of B. Dehay and C. Kubisch (Dehay et al., 2012a, 2012b).

Endocytosis Assays

Reagents were CTb-FITC Sigma C1655, hmw dextran AF647 (Life Technologies; anionic fixable), transferrin AF488 (Life Technologies T13342), soluble cholesterol (12.5 μg/ml, Sigma, C4951; Kozik et al., 2013), bafilomycin A1 (100 nM with vol/vol matched DMSO control, Sigma, B1793), Nigericin (5 μM, Sigma N7143), and Filipin (25 μg/ml, Sigma F9765 and F4767). In brief, cells were plated out the day before in 24-well plates with a rat tail-coated collagen-coated coverslip (BD). At time zero, we removed the media from the well and added the substrate-containing solution. We then returned the plate to the incubator and removed and processed the coverslips at the indicated times post-addition; these time points were selected after time course optimization experiments. For the CTb and dextran assays, we allowed the samples to incubate for 20 min at 37°C after addition of the substrate-containing media and then washed them twice with room temperature PBS and added 0.5 ml of room temperature 0.25% trypsin. We let it sit for 1 minute, removed trypsin, washed it with cold complete media twice, fixed with cold 0.4% formalin in PBS, and washed it once with PBS. For transferrin, we used a published protocol (Tacheva-Grigorova et al., 2013): we removed the media and washed with cold PBS twice and then incubated for 2 min in cold stripping buffer (150 mM NaCl, 20 mM HEPES, 5 mM KCl, 1 mM $CaCl_2$, 1 mM $MgCl_2$ [pH 5.5]) twice and then washed with cold PBS and fixed with cold formalin in PBS. The stripping buffer removes the surface bound transferrin but does not remove the receptor so that it can be stained for below. With the transferrin entry assay, we co-stained with an antibody against TfR (Purified Mouse Anti-human CD71, BD PharMingen, cat: 555534) as previously described (Tacheva-Grigorova et al., 2013). Cholesterol was depleted from cells as previously described (Subtil et al., 1999) using 10 mM MβCD (Sigma) for 10 min at 37°C. Cholesterol was added to cells using MβCD complexed with cholesterol (Sigma) for 10 min at 37°C.

Viral Entry Assays

Quantification of viral entry was done by measuring the mean intensity of viral staining in each cell as delineated by the corresponding DIC image. The intensity of the background for each image was subtracted from the cell's mean intensity value. Greater or equal to 15 cells were analyzed per condition across each of three independent experiments. The average and SD for the intensity of the cells for each condition was calculated and normalized to the NT negative control condition.

SUPPLEMENTAL INFORMATION

Supplemental Information includes Supplemental Experimental Procedures, seven figures, and seven tables and can be found with this article online at http://dx.doi.org/10.1016/j.celrep.2015.06.076.

AUTHOR CONTRIBUTIONS

A.M.A., J.M. Perreira, G.S., C.C., W.M.M., J.M. Portmann, M.R., and A.L.B. designed experiments, performed experiments, analyzed data, and wrote the manuscript. P.M., M.C.S., W.M.M., R.E.B., A.G., and M.F. designed experiments and analyzed data.

ACKNOWLEDGMENTS

We thank S.J. Elledge and T. Davoli, M.A. Poritz, the ICCB-L (S. Johnston, S. Rudnicki, and D. Wrobel), UMMS (R. Adshead; M. Sanderson; P. Spatrick; Genomics Core, B. Hobbs, C. Barry, L. Benson, T. Brailey). A.L.B. is grateful to Boehringer-Ingelheim Inc., the Burroughs Wellcome Fund, and the NIH (1R01AI091786) for their support.

Received: June 9, 2015
Revised: June 22, 2015
Accepted: June 29, 2015
Published: July 23, 2015

REFERENCES

Adamson, B., Smogorzewska, A., Sigoillot, F.D., King, R.W., and Elledge, S.J. (2012). A genome-wide homologous recombination screen identifies the RNA-binding protein RBMX as a component of the DNA-damage response. Nat. Cell Biol. *14*, 318–328.

Brass, A.L., Huang, I.C., Benita, Y., John, S.P., Krishnan, M.N., Feeley, E.M., Ryan, B.J., Weyer, J.L., van der Weyden, L., Fikrig, E., et al. (2009). The IFITM proteins mediate cellular resistance to influenza A H1N1 virus, West Nile virus, and dengue virus. Cell *139*, 1243–1254.

Buehler, E., Chen, Y.C., and Martin, S. (2012). C911: A bench-level control for sequence specific siRNA off-target effects. PLoS ONE *7*, e51942.

Che, Z., Olson, N.H., Leippe, D., Lee, W.M., Mosser, A.G., Rueckert, R.R., Baker, T.S., and Smith, T.J. (1998). Antibody-mediated neutralization of human rhinovirus 14 explored by means of cryoelectron microscopy and X-ray crystallography of virus-Fab complexes. J. Virol. *72*, 4610–4622.

Cherry, S., Doukas, T., Armknecht, S., Whelan, S., Wang, H., Sarnow, P., and Perrimon, N. (2005). Genome-wide RNAi screen reveals a specific sensitivity of IRES-containing RNA viruses to host translation inhibition. Genes Dev. *19*, 445–452.

Cherry, S., Kunte, A., Wang, H., Coyne, C., Rawson, R.B., and Perrimon, N. (2006). COPI activity coupled with fatty acid biosynthesis is required for viral replication. PLoS Pathog. *2*, e102.

Dehay, B., Martinez-Vicente, M., Ramirez, A., Perier, C., Klein, C., Vila, M., and Bezard, E. (2012a). Lysosomal dysfunction in Parkinson disease: ATP13A2 gets into the groove. Autophagy *8*, 1389–1391.

Dehay, B., Ramirez, A., Martinez-Vicente, M., Perier, C., Canron, M.H., Doudnikoff, E., Vital, A., Vila, M., Klein, C., and Bezard, E. (2012b). Loss of P-type ATPase ATP13A2/PARK9 function induces general lysosomal deficiency and leads to Parkinson disease neurodegeneration. Proc. Natl. Acad. Sci. USA *109*, 9611–9616.

Echeverri, C.J., Beachy, P.A., Baum, B., Boutros, M., Buchholz, F., Chanda, S.K., Downward, J., Ellenberg, J., Fraser, A.G., Hacohen, N., et al. (2006). Minimizing the risk of reporting false positives in large-scale RNAi screens. Nat. Methods *3*, 777–779.

Economopoulou, M.A., Fragoulis, E.G., and Sideris, D.C. (2007). Molecular cloning and characterization of the human RNase kappa, an ortholog of Cc RNase. Nucleic Acids Res. *35*, 6389–6398.

Feeley, E.M., Sims, J.S., John, S.P., Chin, C.R., Pertel, T., Chen, L.M., Gaiha, G.D., Ryan, B.J., Donis, R.O., Elledge, S.J., and Brass, A.L. (2011). IFITM3 inhibits influenza A virus infection by preventing cytosolic entry. PLoS Pathog. *7*, e1002337.

Feng, H., Cheng, T., Pavlos, N.J., Yip, K.H., Carrello, A., Seeber, R., Eidne, K., Zheng, M.H., and Xu, J. (2008). Cytoplasmic terminus of vacuolar type proton pump accessory subunit Ac45 is required for proper interaction with V(0) domain subunits and efficient osteoclastic bone resorption. J. Biol. Chem. *283*, 13194–13204.

Fuchs, R., and Blaas, D. (2012). Productive entry pathways of human rhinoviruses. Adv. Virol. *2012*, 826301.

Hiesinger, P.R., Fayyazuddin, A., Mehta, S.Q., Rosenmund, T., Schulze, K.L., Zhai, R.G., Verstreken, P., Cao, Y., Zhou, Y., Kunz, J., and Bellen, H.J. (2005). The v-ATPase V0 subunit a1 is required for a late step in synaptic vesicle exocytosis in Drosophila. Cell *121*, 607–620.

Jansen, E.J., Holthuis, J.C., McGrouther, C., Burbach, J.P., and Martens, G.J. (1998). Intracellular trafficking of the vacuolar H+-ATPase accessory subunit Ac45. J. Cell Sci. *111*, 2999–3006.

Jansen, E.J., van Bakel, N.H., Olde Loohuis, N.F., Hafmans, T.G., Arentsen, T., Coenen, A.J., Scheenen, W.J., and Martens, G.J. (2012). Identification of domains within the V-ATPase accessory subunit Ac45 involved in V-ATPase transport and Ca2+-dependent exocytosis. J. Biol. Chem. *287*, 27537–27546.

John, S.P., Chin, C.R., Perreira, J.M., Feeley, E.M., Aker, A.M., Savidis, G., Smith, S.E., Elia, A.E., Everitt, A.R., Vora, M., et al. (2013). The CD225 domain of IFITM3 is required for both IFITM protein association and inhibition of influenza A virus and dengue virus replication. J. Virol. *87*, 7837–7852.

Johnston, S.L., Pattemore, P.K., Sanderson, G., Smith, S., Lampe, F., Josephs, L., Symington, P., O'Toole, S., Myint, S.H., Tyrrell, D.A., et al. (1995). Community study of role of viral infections in exacerbations of asthma in 9-11 year old children. BMJ *310*, 1225–1229.

Kirchhausen, T., Owen, D., and Harrison, S.C. (2014). Molecular structure, function, and dynamics of clathrin-mediated membrane traffic. Cold Spring Harb. Perspect. Biol. *6*, a016725.

Kiritsi, M.N., Fragoulis, E.G., and Sideris, D.C. (2012). Essential cysteine residues for human RNase κ catalytic activity. FEBS J. *279*, 1318–1326.

Kozik, P., Hodson, N.A., Sahlender, D.A., Simecek, N., Soromani, C., Wu, J., Collinson, L.M., and Robinson, M.S. (2013). A human genome-wide screen for regulators of clathrin-coated vesicle formation reveals an unexpected role for the V-ATPase. Nat. Cell Biol. *15*, 50–60.

Luo, B., Cheung, H.W., Subramanian, A., Sharifnia, T., Okamoto, M., Yang, X., Hinkle, G., Boehm, J.S., Beroukhim, R., Weir, B.A., et al. (2008). Highly parallel identification of essential genes in cancer cells. Proc. Natl. Acad. Sci. USA *105*, 20380–20385.

Marshansky, V. (2007). The V-ATPase a2-subunit as a putative endosomal pH-sensor. Biochem. Soc. Trans. *35*, 1092–1099.

Marshansky, V., Rubinstein, J.L., and Grüber, G. (2014). Eukaryotic V-ATPase: novel structural findings and functional insights. Biochim. Biophys. Acta *1837*, 857–879.

Seemungal, T., Harper-Owen, R., Bhowmik, A., Moric, I., Sanderson, G., Message, S., Maccallum, P., Meade, T.W., Jeffries, D.J., Johnston, S.L., and Wedzicha, J.A. (2001). Respiratory viruses, symptoms, and inflammatory markers in acute exacerbations and stable chronic obstructive pulmonary disease. Am. J. Respir. Crit. Care Med. *164*, 1618–1623.

Simmonds, P., McIntyre, C., Savolainen-Kopra, C., Tapparel, C., Mackay, I.M., and Hovi, T. (2010). Proposals for the classification of human rhinovirus species C into genotypically assigned types. J. Gen. Virol. *91*, 2409–2419.

Subtil, A., Gaidarov, I., Kobylarz, K., Lampson, M.A., Keen, J.H., and McGraw, T.E. (1999). Acute cholesterol depletion inhibits clathrin-coated pit budding. Proc. Natl. Acad. Sci. USA *96*, 6775–6780.

Supek, F., Supekova, L., Mandiyan, S., Pan, Y.C., Nelson, H., and Nelson, N. (1994). A novel accessory subunit for vacuolar H(+)-ATPase from chromaffin granules. J. Biol. Chem. *269*, 24102–24106.

Tacheva-Grigorova, S.K., Santos, A.J., Boucrot, E., and Kirchhausen, T. (2013). Clathrin-mediated endocytosis persists during unperturbed mitosis. Cell Rep. *4*, 659–668.